Numerically Exact Simulation of Photodoped Mott Insulators

Fabian Künzel,[1] André Erpenbeck,[2] Daniel Werner,[3] Enrico Arrigoni,[3] Emanuel Gull,[2] Guy Cohen,[4,5] and Martin Eckstein[1,6]

[1]*Institute of Theoretical Physics, University of Hamburg, 20355 Hamburg, Germany*
[2]*Department of Physics, University of Michigan, Ann Arbor, Michigan 48109, USA*
[3]*Institute of Theoretical and Computational Physics, Graz University of Technology, 8010 Graz, Austria*
[4]*The Raymond and Beverley Sackler Center for Computational Molecular and Materials Science, Tel Aviv University, Tel Aviv 6997801, Israel*
[5]*School of Chemistry, Tel Aviv University, Tel Aviv 6997801, Israel*
[6]*The Hamburg Centre for Ultrafast Imaging, Hamburg, Germany*

(Received 23 November 2023; accepted 20 March 2024; published 23 April 2024)

A description of long-lived photodoped states in Mott insulators is challenging, as it needs to address exponentially separated timescales. We demonstrate how properties of such states can be computed using numerically exact steady state techniques, in particular, the quantum Monte Carlo algorithm, by using a time-local ansatz for the distribution function with separate Fermi functions for the electron and hole quasiparticles. The simulations show that the Mott gap remains robust to large photodoping, and the photodoped state has hole and electron quasiparticles with strongly renormalized properties.

DOI: 10.1103/PhysRevLett.132.176501

Introduction.—Short light pulses provide intriguing avenues to manipulate material properties on ultrafast timescales [1–3]. Mott insulators are particularly interesting in this regard [4], because a zoo of complex orders can emerge from a perturbed Mott phase. A versatile route toward the generation of nonthermal phases involves photodoping, i.e., the creation of charge carriers such as doublons (doubly occupied sites) and holes in a single-orbital Mott insulator. With increasing gap, carrier recombination becomes exponentially slow [5–7], so that doublon and hole densities are approximately conserved over extended periods. Energy dissipation into the spin and phonon background eventually yields a cold state akin to electron-hole liquids in semiconductors [8]. Such cold photodoped phases in correlated electron systems may undergo metal insulator transitions and band reconstruction [9–14] and potentially even manifest superconducting instabilities [15–18].

Dynamical mean field theory (DMFT) [19] and its extensions [20,21] are a powerful approach to study Mott materials. The main challenge in extending these methods to the time domain is the solution of a quantum impurity model. Real-time nonequilibrium DMFT simulations [22,23] based on numerically exact quantum Monte Carlo (QMC) [24–26] or matrix-product states [27,28] have been limited to short times, hindering the study of cold photodoped states. Presently, state-of-the-art methods to study photodoped Mott insulators are perturbative variants of the strong-coupling expansion [29–31], notably the noncrossing approximation (NCA), which unfortunately is least reliable in the most relevant metallic regime. For example, in equilibrium, NCA simulations are known to overestimate the Mott gap. This raises skepticism regarding predictions concerning photodoped phases, which hinge on the assumption that the Mott gap is resilient to photodoping. Conversely, significant advance has been made with nonperturbative techniques aimed at the nonequilibrium steady state, through the auxiliary master equation formalism (AMEA) [32] and, more recently, the steady state variant [33] of the inchworm QMC algorithm [34], a high-order stochastic evaluation of the self-consistent strong-coupling expansion.

In this Letter, we aim to use such potentially numerically exact steady state solvers to investigate slowly evolving (quasisteady) photodoped states. Previously, quasisteady photodoped states have been modeled as an equilibrium state of an approximate large-U Hamiltonian which *exactly* conserves the doublon and hole densities [17] and, following ideas introduced in [35], by maintaining the nearly conserved doublon and hole densities by external charge reservoirs [36,37]. Here we introduce an approach that is not restricted to large U and does not alter the system by additional reservoirs. As in quantum kinetic equations [38,39], we take the distribution function $F(\omega, t)$ to be a dynamical variable. The nonperturbative steady state solvers mentioned above can be used to solve the many-body problem with any given distribution function $F_{\text{steady}}(\omega)$. The equilibrium state is a special case where fluctuation-dissipation relations guarantee that $F_{\text{steady}}(\omega)$ is equal to the Fermi function $f(\omega)$. One can therefore introduce a time-local-F ansatz (TLFA), taking the steady state solution with $F(\omega, t) = F_{\text{steady}}(\omega)$ as an approximate description of the

slowly evolving state around time t. Below, we validate the accuracy of the TLFA through real-time simulations and use the ansatz to simulate complex photodoped phases with nonperturbative techniques.

Model.—We consider the one-band Hubbard model at half filling, with Hamiltonian

$$H = -\tilde{t}_0 \sum_{\sigma\langle i,j\rangle} c^\dagger_{\sigma i} c_{\sigma j} + U \sum_i n_{i\uparrow} n_{i\downarrow} - \frac{U}{2} \sum_{\sigma i} n_{i\sigma}. \quad (1)$$

Here, $c^{(\dagger)}_{\sigma i}$ are electronic annihilation (creation) operators at site i and spin σ, $n_{i\sigma} = c^\dagger_{\sigma i} c_{\sigma i}$, U is the Coulomb repulsion, and $\tilde{t}_0$ is the hopping amplitude between nearest-neighbor sites $\langle i, j\rangle$. We solve this system by means of nonequilibrium DMFT [22] on the Bethe lattice with coordination number $z \to \infty$ and hopping $\tilde{t}_0 = t_0/\sqrt{z}$. We use a hopping $t_0 = \sqrt{2}$ (bandwidth 8) and $\hbar = 1$, i.e., all energies are measured in $t_0/\sqrt{2}$ and times are measured in units of $\sqrt{2}/t_0$. To describe the energy dissipation, we include an external bosonic bath via a phonon self-energy $\Sigma_{\rm ph}(t, t') = g^2 G(t, t') D_{\rm bath}(t, t')$, with coupling strength $g^2 = 0.5$ and a linear density of states $D_{\rm bath}(\omega) = (\omega/\omega_c^2) e^{-(\omega/\omega_c)}$ [40,41]. The cutoff $\omega_c = 0.2 \ll U$ is chosen such that only kinetic energy relaxation of doublons and holes is possible, while direct recombination via phonon emission is not.

TLFA.—For validating the TLFA, we solve the model in Eq. (1) in real time in a setting similar to Ref. [42], using DMFT + NCA within the NESSi simulation package [43]. We start from the Mott phase ($U = 8$) at a high initial temperature $T_i = 2$ and monitor the evolution as energy is dissipated to the bosonic bath at lower temperature $T_{\rm bath} = 1/12.5$. Such a temperature quench is convenient to initiate the dynamics with a given density of doublons and holes, but an analogous long-time dynamics is expected if the initial state population is generated by a short pulse [42]. The doublon-hole recombination after the quench is evident in Fig. 1(a) through the slow decay of the double occupancy $d(t) = \langle n_\uparrow(t) n_\downarrow(t)\rangle$. The kinetic energy $K(t)$ shows a much faster initial drop, which reflects the initial intraband relaxation process due to the phonon bath and a slower increase associated to doublon-holon recombination. This temporal separation is more pronounced for larger gaps [44].

To analyze spectral and distribution functions, we perform a partial Fourier transformation (Wigner transform) of the real-time Green's functions $G^{R,<}(\omega, t) = \int ds e^{i\omega s} G^{R,<}(t + s/2, t - s/2)$ at average time t, using a fixed window $|s| \le 150$ for the relative time s. The spectral function and distribution function are then given by $A(\omega,t) = -\frac{1}{\pi}{\rm Im}\{G^R(\omega,t)\}$ and $F(\omega,t) = -\frac{1}{2}{\rm Im}\{G^<(\omega,t)\}/{\rm Im}\{G^R(\omega,t)\}$, respectively. The spectral function [Fig. 1(b)] starts from two Hubbard bands with a partially filled gap due to the high initial temperature. As the kinetic energy of the doublons relaxes within a few tens of inverse hoppings, the occupied density of states $A^<(\omega, t) \equiv F(\omega, t) A(\omega, t)$ concentrates at the lower band edge of the upper Hubbard band. At the same time, two peaks emerge in the spectrum at the edges of the Mott gap, which indicate the simultaneous presence of doublon and hole quasiparticles [18,40,42]. Correspondingly, the distribution function develops two separate quasiparticle chemical potentials for the hole and doublon charge carriers [Fig. 1(c)]. These spectral characteristics slowly relax back to equilibrium as doublons and holes recombine.

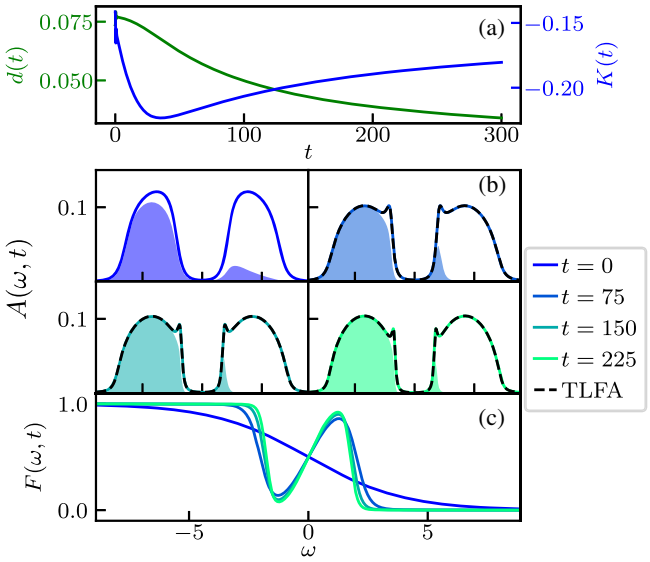

FIG. 1. Time evolution of the photoexcited state, initially prepared at $T_i = 2.0$. (a) Expectation value of the double occupancy $d(t)$ (left axis) an kinetic energy $K(t)$ (right axis). (b) Spectral function $A(\omega, t)$ (solid line) and occupied density of states $A^<(\omega, t)$ (shaded area) for different representative times. (c) Distribution function $F(\omega, t)$ at different times. Dashed lines in (b) show the spectra obtained from the TLFA, with the corresponding distribution function taken from (c).

To implement the TLFA, we extract the function $F(\omega, t)$ at a particular time t and determine a nonequilibrium steady state solution with distribution function $F_{\rm steady}(\omega) = F(\omega, t)$. In practice, we solve the DMFT impurity model with a time-translationally invariant hybridization function whose spectral (retarded) component $\Delta^R(\omega)$ is determined through the DMFT self-consistency, while the lesser component is determined by the given distribution function $F_{\rm steady}(\omega)$, i.e., $\Delta^<(\omega) = -\frac{1}{2} F_{\rm steady}(\omega) {\rm Im}\Delta^R(\omega)$. The resulting spectral functions $A_{\rm TLFA}(\omega)$ are shown by dashed lines in Fig. 1(b). They almost perfectly reproduce the real-time spectra, i.e., the distribution function $F(\omega, t)$ characterizes the system at time t, without further dependence on the history.

Nonequilibrium steady state spectral functions in the photodoped system.—The above validation motivates us to use the TLFA to obtain the spectral function of photodoped

systems using the numerically exact steady state inchworm QMC algorithm. Figure 1(c) suggests to adopt an ansatz for the distribution function, which interpolates between Fermi functions $f(\omega \mp \mu_{\rm ex}, T)$ with generalized chemical potentials $\pm\mu_{\rm ex}$ for the electronlike ($\omega > 0$) and holelike ($\omega < 0$) side, respectively. More precisely, $F_{T,\mu_{\rm ex}}(\omega) = \Theta_\alpha(\omega) f(\omega + \mu_{\rm ex}, T) + [1 - \Theta_\alpha(\omega)] f(\omega - \mu_{\rm ex}, T)$, with a smooth step function $\Theta_\alpha(\omega) = 0.5(1 - \tanh(\omega\alpha/2))$. This ansatz also well describes the distribution function observed in earlier simulations [36,42]. The interpolation affects $F_{T,\mu_{\rm ex}}(\omega)$ only within the gap, so that results are largely independent of the parameter α [44]; below we choose $\alpha = \beta$. We then fix a given photodoping density,

$$n_{\rm ex}(T, \mu_{\rm ex}) = -\frac{1}{\pi} \int_0^\infty d\omega\, F_{T,\mu_{\rm ex}}(\omega) \mathrm{Im}\{\Delta^R(\omega)\}, \qquad (2)$$

by adapting $\mu_{\rm ex}$. At half filling, spectra and quasiparticle properties are symmetric with respect to hole and doublon excitations.

The inchworm QMC algorithm computes the time-translationally invariant Green's functions $G^{R,<}(t - t')$ from the real-time hybridization function $\Delta^{R,<}(t - t')$. In each DMFT iteration, we transform $G^R(t - t')$ to obtain $G^R(\omega)$, determine the self-consistent $\Delta^R(\omega)$, set $\Delta^<(\omega) = -\frac{1}{2}\mathrm{Im}\Delta^R(\omega) F_{T,\mu_{\rm ex}}(\omega)$, where $\mu_{\rm ex}$ is determined to match condition (2) for a given $n_{\rm ex}$, obtain $\Delta^R(t)$ and $\Delta^<(t)$ from the inverse Fourier transform, and perform the Monte Carlo evaluation of G. For details of the inchworm QMC implementation, we refer to [33]. The convergence of the inchworm QMC data with the DMFT iteration and with the diagrammatic order is analyzed in the Supplementary Material [44]. We note that the DMFT iteration based on the TLFA is easier to converge compared to a conventional steady state setup, where the solution depends on external reservoirs [36,37]. In the latter case, both $\Delta^R(\omega)$ and $\Delta^<(\omega)$ would be determined from independent self-consistency conditions, and the additional Monte Carlo noise in $\Delta^<(\omega)$ slows convergence.

In Fig. 2(a), we compare the spectral function $A(\omega)$ obtained for NCA and the numerically exact inchworm QMC. The main characteristics of the cold photodoped state, which is the simultaneous hole and electron quasiparticle peak, is thereby validated by the numerically exact data. From the spectra we can extract the gap $\Delta_{\rm g}$, see Fig. 2(c). Here, NCA overestimates the gap $\Delta_{\rm g}$ in the photodoped state, consistent with its behavior in equilibrium [45]. Suppressing higher-order diagrams essentially increases the effective interaction strength and leads to a larger gap. Nevertheless, one finds that the gap remains robust at large photodoping $n_{\rm ex}$ even in the numerically exact solution, which is an important finding supporting the stability of photodoped orders.

We also compute NCA and inchworm QMC spectra for a photodoping close to population inversion, see Fig. 3(a).

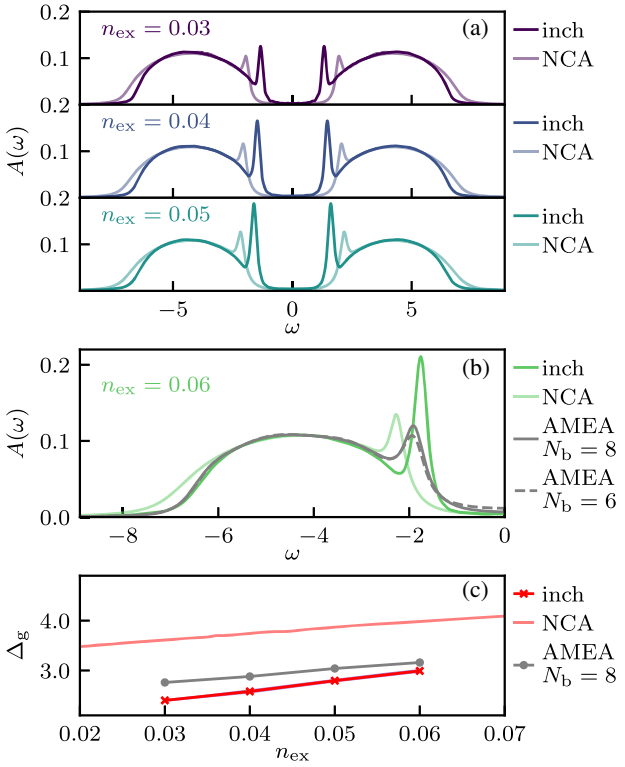

FIG. 2. (a) Comparison of the spectral function $A(\omega)$ for given $n_{\rm ex}$, obtained by inchworm QMC (solid lines) and by NCA (transparent lines), at temperature $T_\Delta = 1/12.5$. (b) Comparison as in (a) with AMEA spectra using six (dashed gray line) and eight bath sites (solid gray line), for $n_{\rm ex} = 0.06$. (c) The Mott gap $\Delta_{\rm g}$ for all three approaches. The gap is defined by the spectral weight reaching 0.057, which is half of the maximum of the equilibrium spectrum. For a visualization of the inchworm QMC error, the mean of five inchworm DMFT iterations is plotted together with the standard deviation (shaded region).

Also in this extreme case, the inchworm code validates the photodoped state and shows characteristic quasiparticle peaks at the outer edges of the Hubbard band as well as a superposition of two separate Fermi functions in the distribution function $F(\omega)$ in Fig. 3(b). This supports the stability of states with large photodoping, which have also been observed in DMFT + NCA simulations of the Hubbard model using other doping protocols [15,46].

The TLFA can also be evaluated with the AMEA, which approximates the impurity problem with hybridization function $\Delta^R(\omega)$ and $\Delta^<(\omega)$ in terms of a finite open system described by $N_{\rm b}$ bath orbitals with additional Lindblad dissipators. For a detailed description of the bath fitting procedure, see Refs. [47,48]. Relatively inexpensive simulations are possible with up to $N_{\rm b} = 8$ sites within a configuration interaction expansion [49]. While one can see in Fig. 2(b) that these data are not yet converged as a function of $N_{\rm b}$, the difference between $N_{\rm b} = 6$ and 8 sites indicates the correct trend. Even simulations with only $N_{\rm b} = 6$ sites provide a significant improvement over the

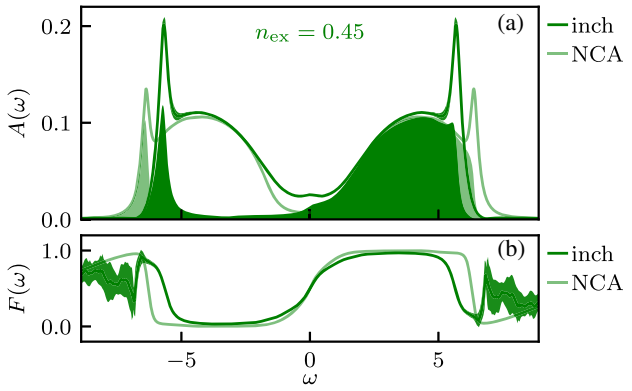

FIG. 3. (a) Spectral function $A(\omega)$ at $n_{ex} = 0.45$, obtained with inchworm QMC (solid lines) and NCA (transparent lines), at temperature $T_\Delta = 1/12.5$. The colored areas denote the occupied spectrum $A^<(\omega)$. (b) Comparison of the inchworm QMC (solid lines) and NCA (transparent lines) distribution function $F(\omega)$ at $n_{ex} = 0.45$ and temperature $T_\Delta = 1/12.5$. The mean of five inchworm DMFT iterations is plotted together with the standard deviation (shaded region).

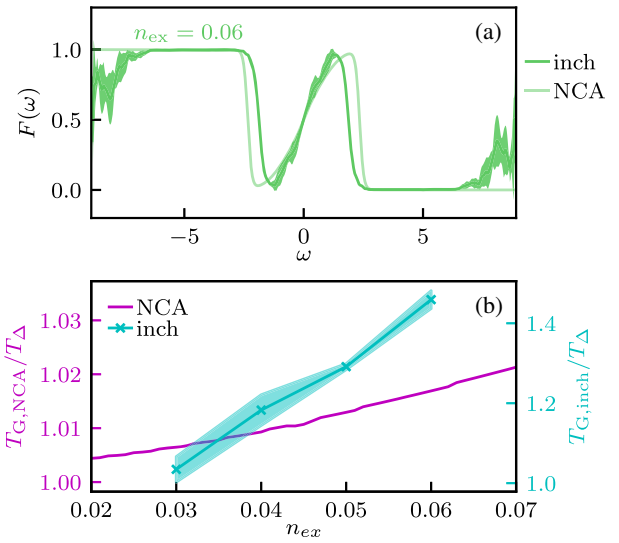

FIG. 4. (a) Distribution function $F(\omega)$ at $n_{ex} = 0.06$, obtained with inchworm QMC (solid lines) and NCA (transparent lines), at temperature $T_\Delta = 1/12.5$. (b) Effective temperature $T_{G,NCA}/T_\Delta$ (left axis) and $T_{G,inch}/T_\Delta$ (right axis) of the quasiparticle excitations using the two methods in relation to T_Δ. For a visualization of the Monte Carlo error, the mean of five inchworm DMFT iterations is plotted together with the standard deviation (shaded region).

NCA simulation regarding the size of the gap and accurately capture the high-energy behavior of the spectra.

For the results presented here, we used an universal ansatz for $F_{steady}(\omega)$, whose form is motivated by previous real-time simulations. An interesting question is if one can validate that this ansatz corresponds to an actual long-lived state. To answer this question, one could compute the time evolution of this state using quantum Boltzmann equations (QBEs) [38]. The latter can be formulated as an evolution equation $\partial_t F(\omega, t) = I[F(\omega, t)]$ for F, where the scattering integral $I[F]$ is determined in terms of the self-energy $\Sigma_{TLFA}[F]$ obtained from a TLFA. An infinitely long-lived state would correspond to a case in which the distribution functions of all quantities (G, Δ, Σ) coincide, and the dynamics within the QBE is driven by the difference in distribution functions. While solving the QBE with AMEA or inchworm QMC is beyond the scope of the present work, a useful quantity to analyze is therefore the difference between F_Δ and F, which is obtained from the computed Green's function.

In Fig. 4(a), we show an example of the distribution F. To quantify how it differs from F_Δ, we extract a temperature T_G from linear fits of the form $-(\omega - \mu_{ex,G})/T_G$ to the function $\log\{F(\omega)/(1 - F(\omega))\}$ in the vicinity of the quasiparticle peak. Figure 4(b) shows that T_G is consistently larger than T_Δ. The difference is larger in the inchworm results (but still comparable in magnitude), which is expected as the smaller gap would imply a faster dynamics, so that the state found by the TLFA has a shorter lifetime and eventually thermalizes.

Conclusion.—Optically excited Mott insulators exhibit slowly evolving quasisteady photodoped states that are challenging to describe theoretically. In this Letter, we have demonstrated how properties of these long-lived photodoped states can be accessed with numerically exact techniques, by using a time-local ansatz for the electronic distribution function. We have validated the consistency of this ansatz upon comparison with real-time simulations in a quenched Hubbard model. Employing a universal form of the distribution function, we directly calculate photodoped Mott spectra for various photoexcitation levels using steady state NCA, inchworm QMC, and AMEA, providing a direct comparison of the methods and novel insights about the validity and reliability of the approximations made in the NCA method. The resulting photodoped spectra can be converged in a wide range of doping densities, and the Mott gap remains robust up to large photodopings for all of the methods. While NCA overestimates the gap, AMEA shows a trend toward the direction of the numerically exact inchworm QMC method. Inchworm QMC is highly accurate at all energies and produces sharp quasiparticle peaks as well as a clean gap. In comparison, AMEA is computationally much less expensive, while providing reasonably accurate values for the gap size, peak positions, and high-energy behavior. However, it introduces a spurious broadening that makes the gap and the peaks less sharp. These findings indicate that nonequilibrium steady state formalisms can be used to directly access quasistable photodoped states in Mott insulators, allowing a numerically exact exploration of photodoping at previously inaccessible experimentally relevant timescales. Furthermore, by integrating the steady state ansatz with QBE schemes, they open up new avenues for characterizing the slow dynamics

of Mott insulators. This approach has the potential to extend into time scales far beyond the capabilities of existing real-time simulations.

We thank Jan Lotze, Jiajun Li, and Philipp Werner for useful discussions. F. K. and M. E. were funded by the Deutsche Forschungsgemeinschaft through QUAST-FOR5249–449872909 (Project P6). Until August 2023, A. E. was funded by the Deutsche Forschungsgemeinschaft —453644843. A. E., starting on September 2023, and E. G. were supported by the U.S. Department of Energy, Office of Science, Office of Advanced Scientific Computing Research and Office of Basic Energy Sciences, Scientific Discovery through Advanced Computing (SciDAC) program under Award No. DESC0022088. G. C. acknowledges support by the Israel Science Foundation (Grants No. 2902/21 and No. 218/19) and by the PAZY foundation (Grant No. 318/78). E. A. and D. W. acknowledge funding by the Austrian Science Fund (FWF) [Grant DOI: 10.55776/P33165] and by NaWi Graz. Some computations were performed on the HPC-Cluster of the PHYSnet-Rechenzentrum University of Hamburg and the Vienna Scientific Cluster. The remaining computations used resources of the National Energy Research Scientific Computing Center (NERSC), a DOE Office of Science User Facility supported by the Office of Science of the U.S. Department of Energy under Contract No. DE-AC02-05CH11231 using NERSC award BES-ERCAP0021805.

[1] D. N. Basov, R. D. Averitt, and D. Hsieh, Nat. Mater. **16**, 1077 (2017).
[2] C. Giannetti, M. Capone, D. Fausti, M. Fabrizio, F. Parmigiani, and D. Mihailovic, Adv. Phys. **65**, 58 (2016).
[3] A. de la Torre, D. M. Kennes, M. Claassen, S. Gerber, J. W. McIver, and M. A. Sentef, Rev. Mod. Phys. **93**, 041002 (2021).
[4] Y. Murakami, D. Golež, M. Eckstein, and P. Werner, arXiv:2310.05201.
[5] A. Rosch, D. Rasch, B. Binz, and M. Vojta, Phys. Rev. Lett. **101**, 265301 (2008).
[6] R. Sensarma, D. Pekker, E. Altman, E. Demler, N. Strohmaier, D. Greif, R. Jördens, L. Tarruell, H. Moritz, and T. Esslinger, Phys. Rev. B **82**, 224302 (2010).
[7] Z. Lenarčič and P. Prelovšek, Phys. Rev. Lett. **111**, 016401 (2013).
[8] L. V. Keldysh, Contemp. Phys. **27**, 395 (1986).
[9] M. Sandri and M. Fabrizio, Phys. Rev. B **91**, 115102 (2015).
[10] Z. He and A. J. Millis, Phys. Rev. B **93**, 115126 (2016).
[11] D. Wegkamp, M. Herzog, L. Xian, M. Gatti, P. Cudazzo, C. L. McGahan, R. E. Marvel, R. F. Haglund, A. Rubio, M. Wolf, and J. Stähler, Phys. Rev. Lett. **113**, 216401 (2014).
[12] G. Lantz, B. Mansart, D. Grieger, D. Boschetto, N. Nilforoushan, E. Papalazarou, N. Moisan, L. Perfetti, V. L. R. Jacques, D. L. Bolloc'h, C. Laulhé, S. Ravy, J.-P. Rueff, T. E. Glover, M. P. Hertlein, Z. Hussain, S. Song, M. Chollet, M. Fabrizio, and M. Marsi, Nat. Commun. **8**, 13917 (2017).
[13] A. Verma *et al.*, arXiv:2304.02149.
[14] S. Beaulieu, S. Dong, N. Tancogne-Dejean, M. Dendzik, T. Pincelli, J. Maklar, R. P. Xian, M. A. Sentef, M. Wolf, A. Rubio, L. Rettig, and R. Ernstorfer, Sci. Adv. **7**, eabd9275 (2021).
[15] J. Li, D. Golez, P. Werner, and M. Eckstein, Phys. Rev. B **102**, 165136 (2020).
[16] S. Ray, Y. Murakami, and P. Werner, Phys. Rev. B **108**, 174515 (2023).
[17] Y. Murakami, S. Takayoshi, T. Kaneko, Z. Sun, D. Golez, A. J. Millis, and P. Werner, Commun. Phys. **5**, 23 (2022).
[18] P. Werner, J. Li, D. Golež, and M. Eckstein, Phys. Rev. B **100**, 155130 (2019).
[19] A. Georges, G. Kotliar, W. Krauth, and M. J. Rozenberg, Rev. Mod. Phys. **68**, 13 (1996).
[20] T. A. Maier, M. Jarrell, T. Pruschke, and M. Hettler, Rev. Mod. Phys. **77**, 1027 (2005).
[21] G. Rohringer, H. Hafermann, A. Toschi, A. A. Katanin, A. E. Antipov, M. I. Katsnelson, A. I. Lichtenstein, A. N. Rubtsov, and K. Held, Rev. Mod. Phys. **90**, 025003 (2018).
[22] H. Aoki, N. Tsuji, M. Eckstein, M. Kollar, T. Oka, and P. Werner, Rev. Mod. Phys. **86**, 779 (2014).
[23] J. K. Freericks, V. M. Turkowski, and V. Zlatić, Phys. Rev. Lett. **97**, 266408 (2006).
[24] L. Mühlbacher and E. Rabani, Phys. Rev. Lett. **100**, 176403 (2008).
[25] P. Werner, T. Oka, and A. J. Millis, Phys. Rev. B **79**, 035320 (2009).
[26] M. Eckstein, M. Kollar, and P. Werner, Phys. Rev. Lett. **103**, 056403 (2009).
[27] F. A. Wolf, I. P. McCulloch, and U. Schollwöck, Phys. Rev. B **90**, 235131 (2014).
[28] K. Balzer, F. A. Wolf, I. P. McCulloch, P. Werner, and M. Eckstein, Phys. Rev. X **5**, 031039 (2015).
[29] H. Keiter and J. C. Kimball, Phys. Rev. Lett. **25**, 672 (1970).
[30] P. Coleman, Phys. Rev. B **29**, 3035 (1984).
[31] M. Eckstein and P. Werner, Phys. Rev. B **82**, 115115 (2010).
[32] E. Arrigoni, M. Knap, and W. von der Linden, Phys. Rev. Lett. **110**, 086403 (2013).
[33] A. Erpenbeck, E. Gull, and G. Cohen, Phys. Rev. Lett. **130**, 186301 (2023).
[34] G. Cohen, E. Gull, D. R. Reichman, and A. J. Millis, Phys. Rev. Lett. **115**, 266802 (2015).
[35] F. Lange, Z. Lenarčič, and A. Rosch, Nat. Commun. **8**, 15767 (2017).
[36] J. Li and M. Eckstein, Phys. Rev. B **103**, 045133 (2021).
[37] H. Atanasova, A. I. Lichtenstein, and G. Cohen, Phys. Rev. B **101**, 174316 (2020).
[38] A. Picano, J. Li, and M. Eckstein, Phys. Rev. B **104**, 085108 (2021).
[39] A. Kamenev, *Field Theory of Non-Equilibrium Systems* (Cambridge University Press, Cambridge, England, 2011).
[40] M. Eckstein and P. Werner, Phys. Rev. Lett. **110**, 126401 (2013).
[41] F. Peronaci, M. Schiró, and O. Parcollet, Phys. Rev. Lett. **120**, 197601 (2018).
[42] N. Dasari, J. Li, P. Werner, and M. Eckstein, Phys. Rev. B **103**, L201116 (2021).

[43] M. Schüler, D. Golez, Y. Murakami, N. Bittner, A. Herrmann, H. U. Strand, P. Werner, and M. Eckstein, Comput. Phys. Commun. **257**, 107484 (2020).
[44] See Supplemental Material at http://link.aps.org/supplemental/10.1103/PhysRevLett.132.176501 for details on the convergence of the inchworm QMC data, as well as on the universality of the ansatz for the distribution function and a real-time simulation for a system with larger Mott gap.
[45] T. Pruschke and N. Grewe, Z. Phys. B **74**, 439 (1989).
[46] P. Werner, J. Li, D. Golež, and M. Eckstein, Phys. Rev. B **100**, 155130 (2019).
[47] A. Dorda, M. Nuss, W. von der Linden, and E. Arrigoni, Phys. Rev. B **89**, 165105 (2014).
[48] A. Dorda, M. Sorantin, W. von der Linden, and E. Arrigoni, New J. Phys. **19**, 063005 (2017).
[49] D. Werner, J. Lotze, and E. Arrigoni, Phys. Rev. B **107**, 075119 (2023).